

Extreme View Synthesis

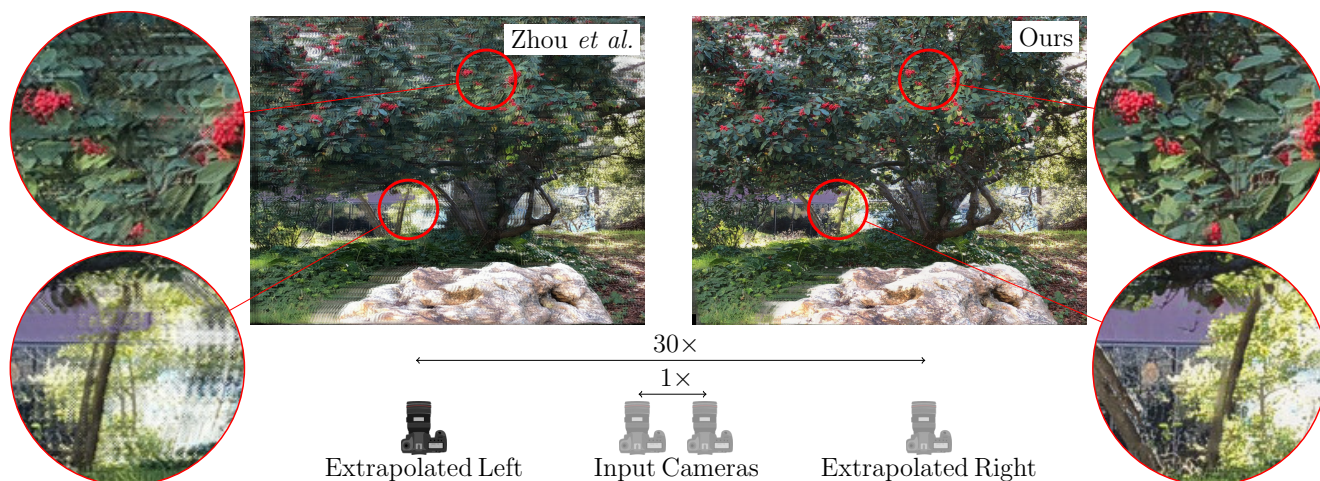
Inchang Choi^{1,2}Orazio Gallo¹Alejandro Troccoli¹Min H. Kim²Jan Kautz¹¹NVIDIA²KAIST

Figure 1: We propose a novel view synthesis method that can generate *extreme* views, *i.e.* images synthesized from a small number of cameras (two in this example) and from significantly different viewpoints. In this comparison with the method by Zhou *et al.* [24], we show the left view from the camera setup depicted below. Even with a baseline magnification of $30\times$, our method produces sharper results.

Abstract

We present *Extreme View Synthesis*, a solution for novel view extrapolation when the number of input images is small. Occlusions and depth uncertainty, in this context, are two of the most pressing issues, and worsen as the degree of extrapolation increases. State-of-the-art methods approach this problem by leveraging explicit geometric constraints, or learned priors. Our key insight is that only by modeling both depth uncertainty and image priors can the extreme cases be solved. We first generate a depth probability volume for the novel view and synthesize an estimate of the sought image. Then, we use learned priors combined with depth uncertainty, to refine it. Our method is the first to show visually pleasing results for baseline magnifications of up to $30\times$.

1. Introduction

The ability to capture visual content and render it from a different perspective, usually referred to as *novel view synthesis*, is a long-standing problem in computer graphics. When appropriately solved, it enables telepresence ap-

plications such as head-mounted virtual and mixed reality, and navigation of remote environments on a 2D screen—an experience popularized by Google Street View. The user content that is uploaded to sharing services at an increasing rate offers a rich source of data for novel view synthesis. However, these collections are generally too sparse to render all the views that may be desired. Synthesis from sparse views is extremely challenging, in particular when generating views creating disocclusions, which is frequently the case when the viewpoint is extrapolated, rather than interpolated, from the input cameras.

Early novel view synthesis methods can generate new images by interpolation either in pixel space [4], or in ray space [16]. More recent approaches use large data collections and learn the new views directly, allowing for small-baseline extrapolation as well [7, 24]. The power of learning-based approaches lies in their ability to leverage useful image priors to fill missing regions or correct for poorly reconstructed ones. However, when the position of the virtual camera differs significantly from that of the inputs, methods that do not use depth information, or use it only implicitly, tend to introduce visible artifacts.

Novel views, then, can be synthesized with geometric methods, which use 3D information explicitly. A typical

approach would use it to warp the input views to the virtual camera, merge them based on a quality measure, and potentially perform some post-processing to attenuate artifacts. The advantage of such methods is that they explicitly leverage geometric constraints. Depth, however, does not come without disadvantages. First and foremost is the problem of occlusions. Second, depth estimation is always subject to a degree of uncertainty. Both of these issues are further exacerbated in the case of extrapolation, as shown in Figure 2. Existing methods deal with uncertainty by propagating reliable depth values to similar pixels [2], or by modeling it [18]. However, these approaches cannot leverage depth to post-process the synthesized images, nor do they use image priors to deal with the unavoidable issues of occlusions and artifacts.

In this paper we focus on *extreme view synthesis*. Extreme are those situation with a small number of input views—as few as two—and in which the novel viewpoint is “pushed” as far as possible from the location of the original views. In their *Stereo Magnification* work, Zhou *et al.* show that high-quality stereo baseline extrapolation is possible up to $4.5\times$ [24]. In the same scenario, our method produces visually pleasing results up to a baseline magnification of $30\times$, as shown in Figure 1.

At a high level, we follow the depth-warp-refine paradigm, but we leverage two key insights to achieve such large extrapolation. First, depth estimation is not always reliable: instead of exact depth estimates, we use depth probability volumes. Second, neural networks can be trained to fix the unavoidable artifacts in the synthesized images by leveraging both learned priors and geometric constraints. By combining these two concepts, our method works for both view interpolation and extreme extrapolation. We show results on a large number of examples in which the virtual camera significantly departs from the original views, even when only two input images are given. To the best of our knowledge, our method is the first to produce visually pleasing results for such extreme view synthesis from unstructured cameras.

2. Related Work

Early methods for novel view synthesis date back several decades [9]. Image interpolation methods, among the first approaches to appear, work by interpolating between corresponding pixels from the input images [4], or between rays in space [16]. The novel view can also be synthesized as a weighted combination of the input cameras, when information about the scene geometry is available [1, 6]. All of these methods generally assume additional information—correspondences, depth, or geometry—to be given.

More recent methods produce excellent results taking only images as an input. This can be done, for instance, by using an appropriate representation of the scene, such

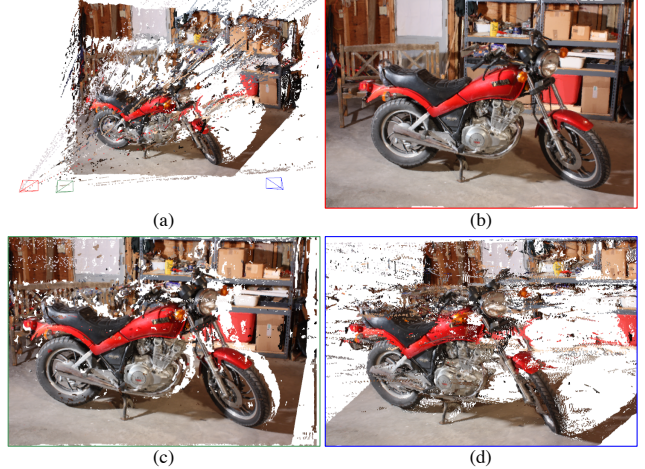


Figure 2: A point cloud (a) and the corresponding images as seen from three cameras (b)-(d). The point cloud was generated from the depth map of the red camera. Note how depth uncertainty causes increasingly large artifacts as the viewpoint moves farther away from the red camera.

as plane sweep volumes, and by learning weights to merge them down into a single image [7]. Further building on the concept layered depth images [10], Zitnick *et al.* developed a high-quality video-based rendering system for dynamic scenes that can interpolate between views [26]. Zhou *et al.* learn a layer-based representation of the scene and the weights necessary to generate novel the view from it [24]. They achieve impressive results, which include small-baseline extrapolation, but they work best when the novel view is close to the input images, *e.g.*, limited translation.

To truly allow the virtual camera to move freely, explicit depth information is necessary: it can be estimated from multiple input images directly and used to warp the input images into the novel view. Kalantari *et al.*, for instance, learn to estimate both disparity and the novel view from the sub-aperture images of a lightfield camera [12]. For larger displacements of the virtual camera, however, depth uncertainty results in noticeable artifacts. Chaurasia *et al.* take accurate but sparse depth and propagate it using super-pixels based on their similarity in image space [2]. Panner and Zhang explicitly model the confidence that a voxel corresponds to empty space or to a physical surface, and use it while performing back-to-front synthesis of the novel view [18].

The ability of deep learning techniques to learn priors has also paved the way to single-image methods. Srinivasan *et al.* learn a light field and depth along each ray from a single image [21]. Zhou *et al.* cast this problem as a prediction of appearance flows, which allows them to synthesize novel views of a 3D object or scene from a single

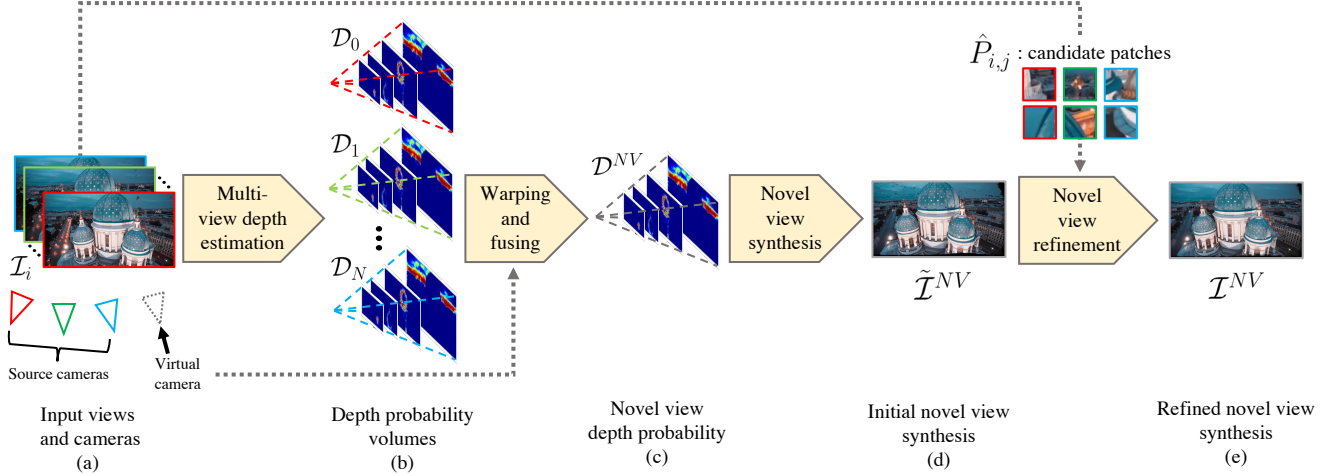


Figure 3: Method overview: from a set of posed input views (a), we generate a set of depth probability volumes for each view (b). Given the novel view camera pose, we create its depth probability volume via warping and fusion of the input depth volumes (c). Next, we synthesize an initial novel view (d), which we refine with a neural network to synthesize the final image (e). Our image refinement is done in a patch-based manner guided by the depth distribution.

observation [25]. From a single image, Xie *et al.* produce stereoscopic images [22], while Tulsiani *et al.* infer a layered representation of the scene.

Our approach differs from existing works for its ability to generate extrapolated images under large viewpoint changes and from as few as two cameras.

3. Overview

Our goal is to synthesize a novel view, \mathcal{I}^{NV} , from N input views, \mathcal{I}_i . A common solution to this problem is to estimate depth and use it to warp and fuse the inputs into the novel view. However, depth estimation algorithms struggle in difficult situations, such as regions around depth discontinuities, causing warping errors and, in turn, artifacts in final image. These issues further worsen when N is small, or \mathcal{I}^{NV} is extrapolated, *i.e.*, when the virtual camera is not on the line between any two input cameras. Rather than using a single depth estimate for a given pixel, our method accounts for the depth’s probability distribution. We first estimate N distributions, one per input view, and combine them to estimate the distribution for the virtual camera, \mathcal{D}^{NV} , Section 4. Based on the combined distribution \mathcal{D}^{NV} , we render the novel view back to front, Section 5. Finally, we refine \mathcal{I}^{NV} at the patch level informed by relevant patches from the input views, which we select based on the depth distribution, Section 6. See Figure 3 for an overview of the proposed pipeline.

4. Estimating the Depth Probability Volume

Several methods exist that estimate depth from multiple images [13, 8], stereo pairs [14, 15], and even single

image [17, 19]. In a particularly relevant work, Huang *et al.* treat depth as a learning-based, multi-class classification problem, thereby estimating a probability distribution along a pixel’s ray [11]. Huang *et al.* output depth probability volumes, $\mathcal{D}_i \in \mathbb{R}^{h \times w \times n_d}$, where $h \times w$ is the resolution of \mathcal{I}_i , and n_d is the number of disparity levels. Traversing this tensor along the disparity dimension gives the probability distribution of each disparity value along $\mathcal{R}_i(x_i, y_i)$, the ray corresponding to pixel (x_i, y_i) in \mathcal{I}_i . We accurately analyzed these depth volumes over a range of different scenarios, and identified a few characteristic behaviors, see Figure 4. For most regions, the method is fairly certain about disparity, and the probability along $\mathcal{R}_i(x, y)$ has single, strong peak around the correct value. At depth discontinuities, the depth is more uncertain. However, rather than expressing this uncertainty by spreading a single peak out, the method produces a multi-modal distribution, with each peak corresponding to one depth layer in the scene. Our method builds on this way of expressing uncertainty.

From the input views we estimate the camera intrinsics and extrinsics with Colmap [20]. For a given scene, we set the closest and farthest disparity levels as the bottom 2 and top 98 depth percentiles respectively, and use $n_d = 100$ uniformly spaced disparity steps. We then use the method by Huang *et al.* to estimate the \mathcal{D}_i ’s. Like Huang *et al.*, we also post-process the \mathcal{D}_i ’s, but we find a more aggressive choice of parameters to perform better.

Each \mathcal{D}_i is computed with respect to the view \mathcal{I}_i , but to warp the input images to \mathcal{I}^{NV} , we need \mathcal{D}^{NV} . We define a simple, yet effective merging strategy for this purpose. For each voxel $\mathcal{D}^{NV}(x, y, d)$ we find the intersecting rays \mathcal{R}_i and average their probability, see Figure 5. The \mathcal{R}_i ’s do not

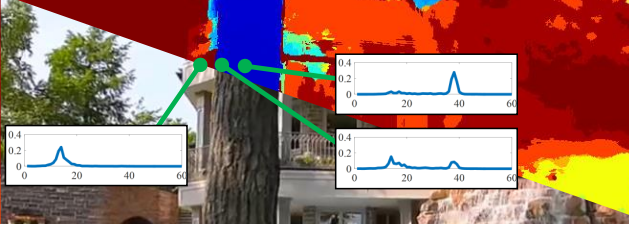


Figure 4: Depth probability distributions along three rays in \mathcal{D} . The disparity shows clear peaks for points that sufficiently distant from a depth discontinuity. Closer to the edge, the inherent uncertainty is captured by the presence of two, lower peaks, one corresponding to the foreground, one to the background.

align with the voxels’ centers, in general. We then use nearest neighbor sampling, which, based on our experiments, yields quality comparable with tri-linear interpolation at a fraction of the cost. After merging all views, we normalize the values along each ray in $\mathcal{D}^{\text{NV}}(x, y)$ to enforce a probability distribution.

5. Synthesis of a Novel View

Using the depth probability volume \mathcal{D}^{NV} , we backward warp pixels from the inputs \mathcal{I}_i and render in a back-to-front fashion an initial estimate of the novel view, $\tilde{\mathcal{I}}^{\text{NV}}$. Specifically, we start from the farthest plane, where $d = 0$, and compute a pixel in the novel view as

$$\tilde{\mathcal{I}}^{\text{NV}}(x, y) \Big|_{d=0} = \mathbf{R} \left(\left\{ \mathcal{I}_i(x_i, y_i) \cdot \mathbb{1}_{\{\mathcal{D}^{\text{NV}}(x, y, 0) > t\}} \right\}_{i=1:N} \right), \quad (1)$$

where $\mathbb{1}$ is the indicator function, and (x_i, y_i) are the coordinates in \mathcal{I}_i that correspond to (x, y) in $\tilde{\mathcal{I}}^{\text{NV}}$. Note that these are completely defined by the cameras’ centers and the plane at d . \mathbf{R} is a function that merges pixels from \mathcal{I}_i weighting them based on the distance of the cameras’ centers, and the angles between the cameras’ principal axes. As we sweep the depth towards a larger disparity d , *i.e.*, closer to the camera, we only overwrite those pixels for which $\mathcal{D}^{\text{NV}}(x, y, d)$ is above threshold. This is expected, since we are rejecting depth estimates that are too uncertain, and we overwrite pixels as we sweep the depth plane from back to front. However, at this stage we are only concerned with generating an initial estimate of the novel view that obeys the geometric constraints available from the depth probability volumes. In the next section we describe how we use the depth probability information to refine $\tilde{\mathcal{I}}^{\text{NV}}$ and remove these artifacts.

6. Image Refinement

Figures 6(a) and (c) show typical artifacts affecting $\tilde{\mathcal{I}}^{\text{NV}}$. Most notably, these include regions that are not rendered,

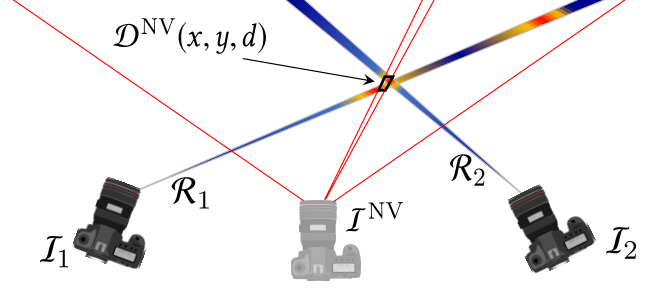


Figure 5: To compute the depth probability associated with a particular voxel in \mathcal{D}^{NV} , we find the intersecting rays from the inputs cameras and average their probability.

either because of occlusions or missing depth information, and the typical “fattening” of edges at depth discontinuities. Moreover, since we render each pixel independently, structures may be locally deformed. We address these artifacts by training a refinement network that works at the patch level. For a pixel p in $\tilde{\mathcal{I}}^{\text{NV}}$, we first extract a 64×64 patch $\tilde{\mathcal{P}}^{\text{NV}}$ around it (for clarity of notation, we omit its dependence on p). A straightforward way to train a refinement network to fix $\tilde{\mathcal{P}}^{\text{NV}}$ would be to train it against the ground truth with an appropriate loss function [23]. However, at inference time, this approach would only leverage image priors and disregard the valuable information the input images carry.

Instead, we scan \mathcal{D}^{NV} to find the likely depths along the ray going out of p , and use them to extract a total of M patches $P_{i,j}$ from the input views \mathcal{I}_i . Consider the case of a ray traveling close to depth discontinuity: as shown in Figure 4, the probability distribution along this ray generally shows two peaks, one corresponding to the foreground and one to the background. As mentioned above, this can result in artifacts at the edge of the depth discontinuity. Rather than fixing this artifacts based only on appearance, we can guide the refinement network with a set of patches extracted from the input views. Away from depth discontinuities, the distribution usually has a single, strong peak, and the synthesized images are generally correct. However, since we warp the pixels independently, slight depth inaccuracy may cause local deformation. Once again, patches from the input views can inform the refinement network about the underlying structure even if the depth is slightly off. This is particularly true since we use overlapping patches.

To minimize view-dependent differences in the patches without causing local deformations, we warp them with the homography induced by the depth plane. For a given disparity $d = \bar{d}$, we compute the warped patch

$$\hat{P}_{i,j} = \mathbf{W}(P_{i,j}, H_{i \rightarrow \text{NV}}^{d=\bar{d}}), \quad (2)$$

where $\mathbf{W}(\cdot, H)$ is an operator that warps a patch based on homography H , and $H_{i \rightarrow \text{NV}}^{d=\bar{d}}$ is the homography induced by

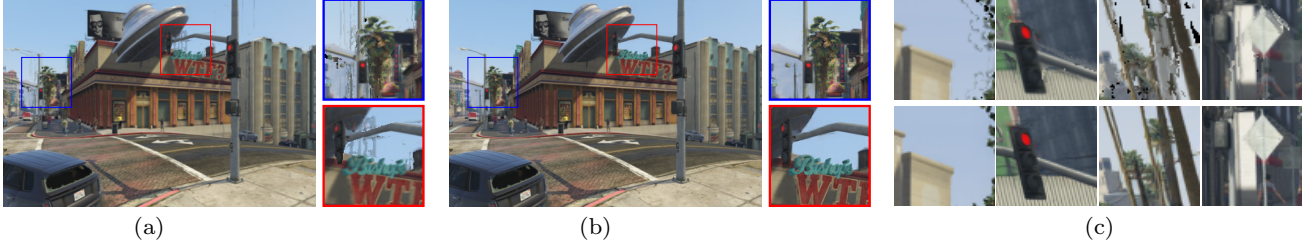


Figure 6: The novel view $\tilde{\mathcal{I}}^{\text{NV}}$, obtained by just warping the inputs, presents several types of artifacts (a). Our refinement network uses the depth probability as well as patches from the input images to fix them (b). More examples of synthesized (top) and refined (bottom) patches are shown in (c).

plane at disparity \bar{d} . This patch selection strategy can be seen as an educated selection of a plane sweep volume [5], where only the few patches that are useful are fed into the refinement network, while the large number of irrelevant patches, which can only confuse it, are disregarded. In the next section we describe our refinement network, as well as details about its training.

We show in Figure 8 a comparison between our network and a network with the same exact number of parameters—the architecture differs only in the fact that it does not have additional patches. It can be observed that the proposed architecture (Figure 8(c) and (f)) can reconstruct local structure even when the single-patch network (Figure 8(b) and (e)) cannot.

The resulting image $\tilde{\mathcal{I}}^{\text{NV}}$ will, in general, presents artifacts and holes, see Figure 6(a).

6.1. Refinement Network

Our refinement strategy, shown in Figure 7, takes a synthesized patch \tilde{P}^{NV} and J warped patches $\hat{P}_{i,j}$ from each input view \mathcal{I}_i . The number of patches contributed to each \tilde{P}^{NV} can change from view to view: because of occlusions, an input image may not “see” a particular patch, or the patch could be outside of its field of view. Moreover, the depth distribution along a ray traveling close to a depth discontinuity may have one peak, or several. As a result, we need to design our refinement network to work with a variable number of patches.

Network Architecture We use a UNet architecture for its proven performance on a large number of vision applications. Rather than training it on a stack of concatenated patches, which would lock us into a specific J , we apply the encoder to each of the available patches independently. We then perform max-pooling over the features generated from all the available patches and we concatenate the result with the features of the synthesized patch, see Figure 7.

The encoder has seven convolutional layers, four of which downsample the data by means of strided convolution. We also use skip connections from the four down-

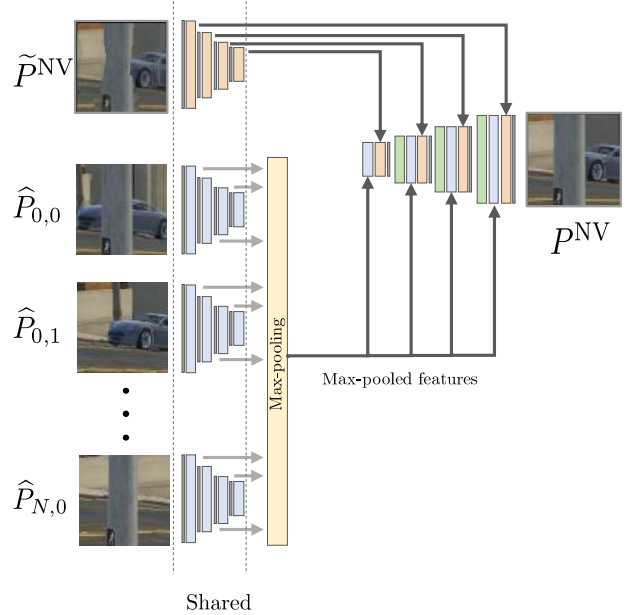


Figure 7: The refinement network takes as input a patch \tilde{P}^{NV} from the synthesized image $\tilde{\mathcal{I}}^{\text{NV}}$, and a variable number of warped patches $\hat{P}_{i,j}$ from each input view \mathcal{I}_i . All patches go through an encoder network. The features of the warped patches are aggregated using max-pooling. Both feature sets are concatenated and used in the decoder that synthesizes the refined patch P^{NV} .

sampling layers of the encoder to the decoder. Each skip connection is a concatenation of the features of the synthesized patch for that layer and a max-pooling operation on the features of the candidate patches at the same layer.

Training To train we use the MVS-Synth dataset [11]. We use the VGG16 loss, which, in our experiments, yields significantly better results compared to ℓ_1 and ℓ_2 . For the details of the loss, we follow the work by Zhuo *et al.* [24]. As for the optimizer we use ADAM. More details about the network and the training are in the [Supplementary](#).

7. Results

In this section we discuss the results our method generates. We recommend to zoom into the images in the electronic version of the paper to better inspect them.

Most methods that perform novel view synthesis focus on interpolation, or a small amount extrapolation, and use a large number of input cameras. To the best of our knowledge, the method of Zhou *et al.* [24] is the first attempt at producing high-quality results for significant baseline magnification. In their paper, Zhou *et al.* show results when magnifying a stereo baseline by a factor of $4.5\times$. While their results are impressive at that magnification, in this paper we push the envelope to *extreme* and show results for $30\times$ magnification of the input baseline. By design, Stereo Magnification can only deal with camera translations in the plane defined by the sensors of the input cameras. To perform a fair comparison, then, we show comparisons on their own stereo data.

Figure 1, and Figure 10 show $30\times$ magnification on stereo pairs of scenes with complicated structure and occlusions. At this magnification level, the results of Zhou *et al.* are affected by strong artifacts. Even in the areas that appear to be correctly reconstructed, such as the head of Mark Twain’s statue in Figure 10(left), a closer inspection reveals a significant amount of blur. Our method generates results that are sharper and present fewer artifacts. We also compare against their method at the magnification level they show, and observe similar results.

The method by Penner and Zhang arguably produces state-of-the-art results for novel view synthesis. However, their code is not available¹ and their problem setting is quite different in that they focus on interpolation and rely on a larger number of input cameras than our method. For completeness, however, we show a comparison against their method in Figure 11. Our reconstruction, which only uses two input cameras, shows a quality that is comparable to their results.

To validate our method more extensively, inspired by the collection strategy implemented by Zhou *et al.* [24], we capture a number of frame sequences from YouTube videos.

A few of the results are shown Figure 9. The leftmost column shows the camera locations for the images shown on the right. The color of the cameras matches the color of the frame around the corresponding image, and gray indicates input cameras. We present results for a number of different camera displacements and scenes, showcasing the strength of our solution. In particular, the first three rows show results using only two cameras as inputs, with the virtual cameras being displaced by several times the baseline between the inputs cameras. The third row shows a dolly-in trajectory (*i.e.* the camera moves towards the scene), which

is a particularly difficult case. Unfortunately, it may be challenging to appreciate the level of extrapolation when comparing images side by side, even when zooming in. However, we also show an animated sequence in Figure 12. To play the sequence, click on the image using a media-enabled reader, such as Adobe Reader.

Furthermore, our method can take any number of input images. The last two rows of Figure 9 show two scenes for which we used four input cameras.

8. Conclusions

We presented a method to synthesize novel views from a set of input cameras. We specifically target *extreme* cases, which are characterized by two factors: small numbers of input cameras, as few as two, and large extrapolation, up to $30\times$ for stereo pairs. To achieve this, we combine traditional geometric constraints with the ability of neural networks to learn image priors. We show results on a several real scenes and camera motions, and for different numbers of input cameras.

Acknowledgments

We thank Abhishek Badki for his help rendering the camera positions for Figure 9.

References

- [1] C. Buehler, M. Bosse, L. McMillan, S. Gortler, and M. Cohen. Unstructured lumigraph rendering. In *ACM Transactions on Graphics (SIGGRAPH)*, 2001.
- [2] G. Chaurasia, S. Duchêne, O. Sorkine-Hornung, and G. Drettakis. Depth synthesis and local warps for plausible image-based navigation. In *ACM Transactions on Graphics*, 2013.
- [3] G. Chaurasia, O. Sorkine, and G. Drettakis. Silhouette-aware warping for image-based rendering. In *Eurographics Symposium on Rendering*, 2011.
- [4] S. E. Chen and L. Williams. View interpolation for image synthesis. In *ACM Transactions on Graphics (SIGGRAPH)*, 1993.
- [5] R. T. Collins. A space-sweep approach to true multi-image matching. In *IEEE Conference on Computer Vision and Pattern Recognition (CVPR)*, 1996.
- [6] P. E. Debevec, C. J. Taylor, and J. Malik. Modeling and rendering architecture from photographs: A hybrid geometry- and image-based approach. In *ACM Transactions on Graphics (SIGGRAPH)*, 1996.
- [7] J. Flynn, I. Neulander, J. Philbin, and N. Snavely. DeepStereo: Learning to predict new views from the world’s imagery. In *IEEE Conference on Computer Vision and Pattern Recognition (CVPR)*, 2016.
- [8] S. Galliani, K. Lasinger, and K. Schindler. Massively parallel multiview stereopsis by surface normal diffusion. In *IEEE International Conference on Computer Vision (ICCV)*, 2015.

¹We attempted to contact the authors but we were unsuccessful.

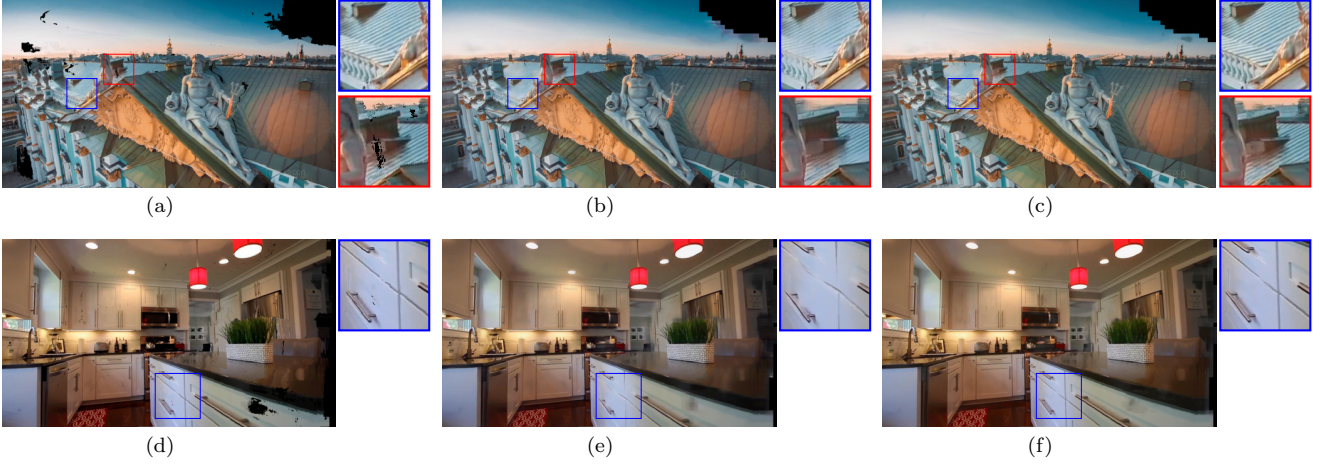


Figure 8: Our refinement network leverages information from relevant patches from the input images. Here (a) and (d) are \tilde{I}^{NV} , (b) and (e) are images created training the network to refine patch only based on image priors, (c) and (f) are our results, which use the patches $\hat{P}_{i,j}$. The structure of the roof is sharper in (c) compared to (b) and (a). The kitchen cabinet is correctly rendered in (f) compared to (d) and (e).



Figure 9: Extreme view synthesis on two-camera inputs and on four-camera inputs. For each row the cameras on the left show the position of the input views (light gray) and virtual views. The color of the pictures' frames matches the color of the corresponding camera on the left. The cameras on the left are rendered at the same scale to facilitate a comparison between the amounts of extrapolation in each case.



Figure 10: Comparison with Stereo Magnification for a $30\times$ baseline magnification. While some unavoidable artifacts are visible in both methods, our results have fewer, less noticeable artifacts, and are generally sharper. Please zoom in for the best viewing experience.



Figure 11: Comparison with Soft3D [18]. (a) A frame generated by Soft3D, which uses all the cameras in the sequence from Chaurasia *et al.* [3], and a frame generated by our method using only two input cameras around the middle of the sequence (b).

Figure 12: Animation showing the first three scenes in Figure 9. **Requires a media-enabled viewer such as Adobe Reader. Click on the image to start the animation.**

[9] N. Greene. Environment mapping and other applications of world projections. In *IEEE Computer Graphics and Applications (CGA)*, 1986.

[10] L.-W. He, J. Shade, S. Gortler, and R. Szeliski. Layered depth images. In *ACM Transactions on Graphics (SIGGRAPH)*, 1998.

[11] P.-H. Huang, K. Matzen, J. Kopf, N. Ahuja, and J.-B. Huang. DeepMVS: Learning multi-view stereopsis. In *IEEE Conference on Computer Vision and Pattern Recognition (CVPR)*, 2018.

[12] N. K. Kalantari, T.-C. Wang, and R. Ramamoorthi. Learning-based view synthesis for light field cameras. In *ACM Transactions on Graphics (SIGGRAPH)*, 2016.

[13] A. Kar, C. Häne, and J. Malik. Learning a multi-view stereo machine. In *Advances in Neural Information Processing Systems (NIPS)*, 2017.

[14] A. Kendall, H. Martirosyan, S. Dasgupta, P. Henry, R. Kennedy, A. Bachrach, and A. Bry. End-to-end learning of geometry and context for deep stereo regression. In *IEEE International Conference on Computer Vision (ICCV)*, 2017.

[15] S. Khamis, S. R. Fanello, C. Rhemann, A. Kowdle, J. P. C. Valentin, and S. Izadi. Stereonet: Guided hierarchical refinement for real-time edge-aware depth prediction. In *European Conference on Computer Vision (ECCV)*, 2018.

[16] M. Levoy and P. Hanrahan. Light field rendering. In *ACM Transactions on Graphics (SIGGRAPH)*, 1996.

[17] Z. Li and N. Snavely. MegaDepth: Learning single-view depth prediction from internet photos. In *IEEE Conference on Computer Vision and Pattern Recognition (CVPR)*, 2018.

[18] E. Penner and L. Zhang. Soft 3D reconstruction for view synthesis. In *ACM Transactions on Graphics (SIGGRAPH)*, 2017.

[19] A. Saxena, S. H. Chung, and A. Y. Ng. Learning depth from single monocular images. In *Advances in Neural Information Processing Systems (NIPS)*, 2006.

[20] J. L. Schönberger and J.-M. Frahm. Structure-from-motion revisited. In *IEEE Conference on Computer Vision and Pattern Recognition (CVPR)*, 2016.

[21] P. P. Srinivasan, T. Wang, A. Sreelal, R. Ramamoorthi, and R. Ng. Learning to synthesize a 4D RGBD light field from a single image. In *IEEE International Conference on Computer Vision (ICCV)*, 2017.

[22] J. Xie, R. Girshick, and A. Farhadi. Deep3D: Fully automatic 2D-to-3D video conversion with deep convolutional neural networks. In *European Conference on Computer Vision (ECCV)*, 2016.

[23] H. Zhao, O. Gallo, I. Frosio, and J. Kautz. Loss functions for image restoration with neural networks. 2017.

[24] T. Zhou, R. Tucker, J. Flynn, G. Fyffe, and N. Snavely. Stereo Magnification: Learning view synthesis using multiplane images. In *ACM Transactions on Graphics (SIGGRAPH)*, 2018.

[25] T. Zhou, S. Tulsiani, W. Sun, J. Malik, and A. A. Efros. View synthesis by appearance flow. In *European Conference on Computer Vision (ECCV)*, 2016.

[26] C. L. Zitnick, S. B. Kang, M. Uyttendaele, S. A. J. Winder, and R. Szeliski. High-quality video view interpolation using a layered representation. In *ACM Transactions on Graphics (SIGGRAPH)*, 2004.